Received: 27 October 2023 | Accepted: 19 April 2024

DOI: 10.1097/HC9.0000000000000473

ORIGINAL ARTICLE

OPEN

Gallbladder dysfunction caused by MYPT1 ablation triggers cholestasis-induced hepatic fibrosis in mice

Ye Wang[1] | **Zhi-Hui Jiang**[1] | **Yu-Wei Zhou**[2] | **Tian-Tian Qiu**[1] | **Han Wang**[1] | **Min-Sheng Zhu**[1] | **Xin Chen**[1] | **Xue-Na Zhang**[1,3,4]

[1]State Key Laboratory of Pharmaceutical Biotechnology, Medical School of Nanjing University, Nanjing, China

[2]Jiangsu Key Laboratory of Molecular Medicine, Department of Otolaryngology Head and Neck Surgery, Nanjing Drum Tower Hospital, Medical School of Nanjing University, Nanjing, China

[3]Jiangsu Key Laboratory for Pharmacology and Safety Evaluation of Chinese Materia Medica, Nanjing University of Chinese Medicine, Nanjing, China

[4]Jinling Pharmaceutical Co., Ltd., Nanjing, China

Correspondence
Min-Sheng Zhu, Medical School of Nanjing University, No.22 Hankou Rd., Gulou District, Nanjing, Jiangsu 210093, China.
Email: zhums@nju.edu.cn

Xin Chen, Medical School of Nanjing University, No.22 Hankou Rd.,Gulou District, Nanjing, Jiangsu 210093, China.
Email: chenxin1028@nju.edu.cn

Xue-Na Zhang, Medical School of Nanjing University, No.22 Hankou Rd., Gulou District, Nanjing, Jiangsu 210093,China.
Email: zhangxn@nju.edu.cn

Abstract

Background: The incidence of gallbladder diseases is as high as 20%, but whether gallbladder diseases contribute to hepatic disorders remains unknown.

Methods: Here, we established an animal model of gallbladder dysfunction and assessed the role of a diseased gallbladder in cholestasis-induced hepatic fibrosis (CIHF).

Results: Mice with smooth muscle-specific deletion of *Mypt1*, the gene encoding the main regulatory subunit of myosin light chain phosphatase (myosin phosphatase target subunit 1 [MYPT1]), had apparent dysfunction of gallbladder motility. This dysfunction was evidenced by abnormal contractile responses, namely, inhibited cholecystokinin 8-mediated contraction and nitric oxide–resistant relaxation. As a consequence, the gallbladder displayed impaired bile filling and biliary tract dilation comparable to the alterations in CIHF. Interestingly, the mutant animals also displayed CIHF features, including necrotic loci by the age of 1 month and subsequently exhibited progressive fibrosis and hyperplastic/dilated bile ducts. This pathological progression was similar to the phenotypes of the animal model with bile duct ligation and patients with CIHF. The characteristic biomarker of CIHF, serum alkaline phosphatase activity, was also elevated in the mice. Moreover, we observed that the myosin phosphatase target subunit 1 protein level was able to be regulated by several reagents, including lipopolysaccharide, exemplifying the risk factors for gallbladder dysfunction and hence CIHF.

Conclusions: We propose that gallbladder dysfunction caused by myosin phosphatase target subunit 1 ablation is sufficient to induce CIHF in mice, resulting in impairment of the bile transport system.

Abbreviations: CCK8, cholecystokinin 8; CIHF, cholestasis-induced hepatic fibrosis; CK19, cytokeratin 19; DEG, differentially expressed gene; KO, knockout; LPS, lipopolysaccharide; MLCP, myosin light chain phosphatase; MYPT1, myosin light chain phosphatase; SMC, smooth muscle cell.

Ye Wang and Zhi-Hui Jiang contribute equally.

Supplemental Digital Content is available for this article. Direct URL citations are provided in the HTML and PDF versions of this article on the journal's website, www.hepcommjournal.com.

INTRODUCTION

The human gallbladder is a small pear-shaped organ composed of epithelial and smooth muscle layers and plays essential roles in digestion by maintaining bile homeostasis. Under fasting conditions, bile produced by the liver is collected and then concentrated in the gallbladder. Upon food intake, via regulated contractile responses of the gallbladder smooth muscle, the stored bile is expelled to the small intestine through the biliary tract so as to digest fat. Under pathological conditions, these processes may be impaired, leading to various gallbladder diseases, such as gallstones, acalculous biliary pain, and gallbladder inflammation.[1,2] The incidence of gallbladder diseases is as high as 20%.[3] Whether gallbladder pathologies induce hepatic disorders remains unclear. Notably, various complications can occur after cholecystectomy (ie, the symptoms of dyspepsia, bile reflux, biliary injury, and increased risks of liver fibrosis, HCC, and gastrointestinal cancer[4–7]), implying involvement of the gallbladder in liver disorders under certain conditions.

Motility is a basic ability of the gallbladder and is mediated by an elaborative process coordinated by contraction/relaxation and spontaneous peristalsis of the gallbladder.[8] Smooth muscle–based motility is highly regulated by hormones (eg, cholecystokinin 8 [CCK8]) and neurotransmitters (eg, acetylcholine and nitric oxide) released from intrinsic neurons and extrinsic sympathetic nerves.[9,10] Additionally, it can be further influenced by physiological and pathological factors such as cholesterol, hydrophobic bile salts and other toxic substances.[11,12] Dysfunctional regulation of gallbladder motility likely impairs hepatic bile homeostasis and hence results in hepatic disorders. However, there are no reports of a causal link between dysfunctional motility of the gallbladder and liver disorders. A key technical reason may be the difficulty in establishing a proper animal model.

Gallbladder motility is driven primarily by the force produced by smooth muscle. Smooth muscle contraction is evoked by depolarization and G protein-coupled receptor-coupled agonists in a calcium (Ca^{2+})-dependent manner.[13,14] Elevated $[Ca^{2+}]_i$ induces myosin regulatory light chain phosphorylation via activation of myosin light chain kinase and potentiates myosin ATPase activity necessary for cross-bridge movement.[15] On the other hand, phosphorylated regulatory light chain can be dephosphorylated by myosin light chain phosphatase (MLCP), which consists of 3 subunits: myosin phosphatase target subunit 1 (MYPT1), a protein phosphatase 1c catalytic core, and a 20 KD kinase with unknown function. MYPT1 binding to the protein phosphatase 1c catalytic subunit is critical for MLCP activity; thus, MYPT1 is a key regulator of Ca^{2+}-sensitized contraction and determines the contractile behaviors of smooth muscles.[16,17] Ablation of MYPT1 may result in abnormal motility of the gastrointestinal tract,[17] and anorectum.[18]

The gallbladder smooth muscle layer consists of a complex interwoven arrangement of muscle cells running in different directions and shares the basic myogenic properties of smooth muscles, although its responsiveness to stimuli is different. CCK8 and acetylcholine are the key stimulators of gallbladder smooth muscle contraction. CCK8 acts presynaptically within gallbladder ganglia to increase the release of acetylcholine from vagal terminals,[8,19] whereas nitric oxide, a primary gas messenger or nerve transmitter, serves as a potent and efficient relaxant of gallbladder smooth muscle in a manner similar to that in other smooth muscles.[20,21] In this study, we observed that MYPT1 also played essential functions in the contractile behaviors of the gallbladder. Deletion of MYPT1 led to dysfunctional motility of the gallbladder. Moreover, this dysfunctional motility might have been exacerbated by gallbladder hyperplasia. Using an MYPT1-deficient mouse line as an animal model of dysfunctional motility of the gallbladder, we assessed the relationship between abnormal motility and hepatic disorder. The results showed that the mutant mice displayed phenotypes similar to those of cholestasis-induced hepatic fibrosis (CIHF),[22–24] thus suggesting that a reduction of MYPT1 expression in smooth muscle might be a pathogenic factor for CIHF-associated diseases.

METHODS

Animals

The knockout (KO) animal model was generated as described.[17] Briefly, floxed mice carrying loxP sites flanking exon 1 of *Mypt1* were crossed with Smooth Muscle Actin-Cre transgenic mice. The resultant animals (*Mypt1*$^{flox/flox}$; Smooth Muscle Actin-Cre, *Mypt1*$^{\triangle SM/\triangle SM}$) displayed smooth muscle-specific deletion of the *Mypt1* gene. All mice were housed under a 12:12-hour light/dark cycle and permitted ad libitum consumption of water and food. All animal procedures were conducted in accordance with the guidelines of the Animal Care and Use Committee of the Model Animal Research Center at Nanjing University (AP#: MZ24). All experiments used both male and female mice. The drugs used have been approved by the FDA (Antibiotics compound Library-L5300, Sellectchem).

Serum biochemistry

Blood samples were collected from mice anesthetized by i.p. injection of avertin. After centrifugation at 6000 rpm for 10 minutes at 4°C, the sera were sampled and frozen at −80°C. Alanine aminotransferase, aspartate transaminase, alkaline phosphatase, and total bilirubin were measured with standard protocols (Wako) using Hitachi 7020 Chemistry Analyzer.

Histological analysis

Liver samples were fixed in 4% paraformaldehyde solution, dehydrated, embedded in paraffin, and cut into 5-μm thick sections. Hepatic necrosis was determined by morphometry on hematoxylin-eosin–stained slides (original magnification, ×10). For semiquantitative assessment of liver fibrosis, sections were stained with Sirius Red (S1020, Solarbio) and photographed, and the positive staining area was calculated. To determine changes in the hepatic bile duct, sections were heated in microwave for antigen retrieval with Citrate Antigen Retrieval Solution (E673001, Sangon Biotech), stained with an antibody against cytokeratin 19 (CK19) (Ab52625, Abcam, 1:2000), and then processed according to the manual of an UltraSensitive SP IHC Kit (KIT-9720, MXB Biotechnologies Co., Ltd.). The cells positive for CK19 were recognized as bile duct epithelial cells. Analysis of the images was performed with Image J software.

Gallbladder samples were fixed in Carnoy solution (R23046, Shanghai yuanye Bio-Technology Co., Ltd.) and embedded in paraffin. These samples were sectioned at a thickness of 5-μm for histological examinations.

Immunofluorescence staining

The gallbladders were isolated, fixed in ice-cold acetone for 10 minutes, and then washed with PBS. Following 20% and 30% sucrose gradient dehydration, the samples were covered with optimum cutting temperature mounting medium and shock-frozen in liquid nitrogen. Cryosections were prepared with a thickness of 10 μm. The nonspecific binding of primary antibodies was blocked by incubation with PBS containing 1% Bovine Serum Albumin and 5% nonimmune goat serum for 1 hour. The blocked slides were incubated overnight with primary antibodies against MYPT1 (22117-1-AP, Proteintech, 1:200) and alpha-smooth muscle actin (Ab7817, Abcam, 1:200). After washing with Phosphate buffrered Saline withTween-20, the slides were then incubated with an Alexa Fluor 555-conjugated goat anti-rabbit antibody (A21428, Sigma, 1:250) or an Alexa Fluor 488–conjugated goat anti-mouse antibody (A11001, Sigma, 1:250) for 1 hour. DAPI (BS097, Biosharp, 1:500) was used for nuclear staining. Immunoreactivity was evaluated using an FV1000 confocal laser scanning microscope system (Olympus).

Determination of hepatic hydroxyproline content

To quantify collagen levels, the amount of hydroxyproline in the left lateral lobe was measured with a hydroxyproline assay kit (BC0250, Solarbio) according to the manufacturer's instructions. The optical density was measured at 560 nm on a microplate reader (BioTek, Synergy H1), and the hydroxyproline content was calculated according to the manufacturer's instructions.

In vitro gallbladder contractility studies

Mice were killed by cervical dislocation, and the gallbladders were removed and immediately placed in cold Krebs-Henseleit solution (NaCl 119 mM, Potassium Chloride 4.7 mM, $NaHCO_3$ 25 mM, KH_2PO4 1.18 mM, $CaCl_2$ 2.5 mM, $MgSO_4(7H_2O)$ 1.17 mM, glucose 11 mM). Each gallbladder was opened from the end of the cystic duct to the base. The gallbladders were washed with Krebs-Henseleit solution to remove residual bile. Force measurements of the bladder strips were performed as described.[25–27] The strips were placed vertically in 10 mL organ baths containing Krebs-Henseleit solution and maintained at 37°C with 95% O_2 and 5% CO_2. Isometric contractions were measured along the longitudinal axis using force transducers (MLT0202; ADInstruments) connected to a PowerLab recording device (ML785, ADInstruments). Prior to recording the force, the strips were equilibrated for at least 30 minutes, and the initial tension was set to 0.1 g. For measuring the contraction in response to depolarization, Krebs solution with 80 mM K^+ solution (NaCl 0.88 mM, Potassium Chloride 122.82 mM, $NaHCO_3$ 25 mM, KH_2PO_4 1.18 mM, $CaCl_2$ 2.5 mM, $MgSO_4$ ($7H_2O$) 1.17 mM, glucose 11 mM) was applied. The contractile response to G protein-coupled receptor agonists was measured by applying CCK8 (1.5 μM) or acetylcholine (100 μM). The relaxation property of the gallbladder muscle strips was measured by stepwise cumulative additions with sodium nitroprusside (10^{-4} to 10^{-2} M) to the precontracted strips by CCK8 (1.5 μM).

Measurement of biliary pressure

Biliary pressure was measured according to a previously described method with modifications.[28] The mice were fasted overnight and sacrificed by cervical dislocation. The distal portion of the cystic duct was ligated, and a saline-filled catheter (29G) threaded through the proximal portion of the duct into the fundus of the gallbladder. The catheter was tied securely in place to prevent leakage of bile. The catheter was then connected to a pressure transducer. The pressure was recorded on a PowerLab recording device (ML785, ADInstruments).

Single-nucleus RNA sequencing and data analysis

To isolate nuclei for single-nucleus RNA sequencing -seq, gallbladder tissues from 16 wild-type and 25 KO mice were used. Nuclei were extracted using GEXSCOPE Nucleus Separation Solution (Singleron Biotechnologies, Nanjing, China) and suspended at $3–4\times10^5$ nuclei/mL in PBS. The suspension was loaded

onto a microfluidic chip (GEXSCOPE Single NucleusRNA-seq Kit, Singleron Biotechnologies) and processed with an Illumina HiSeq X10 instrument for single-nucleus RNA sequencing, producing 150 bp paired-end reads.

Gene expression matrixes were processed using CeleScope v1.9.0 pipeline.[29] Differentially expressed genes (DEGs) were identified via Seurat FindMarkers, focusing on genes expressed in over 10% of the cells in a cluster and an average log (fold change) above 0.25. Cell type were annotated using the SynEcoSys database based on DEGs' canonical markers DEGs' function were explored through Gene Ontology and Kyoto Encyclopedia of Genes and Genomes pathways using the "clusterProfiler" R package 3.16.1,[30] with significances set at *p*-adj values <0.05.

Quantitative real-time PCR

Gallbladders were carefully isolated from mice, the connective tissue was quickly removed, and the gallbladders were frozen in liquid nitrogen. Total RNA was extracted using the TRIzol (9109, Takara Bio) method according to the manufacturer's guidelines. Reverse transcription was performed with HiScriptQ RT SuperMix (R223, Vazyme).The primers were synthesized by GenScript, and their sequences are listed in Supplemental Table S1, http://links.lww.com/HC9/A937. Quantitative PCR was performed on an ABI QuantStudio 5 using Taq Pro Universal SYBR qPCR Master Mix(Q131, Vazyme). Each reaction was carried out in triplicate. The expression levels of the target genes were normalized against those of an endogenous reference gene, β-actin. All data are represented by the fold change ($2^{-\Delta\Delta Ct}$).

Western blot analysis

Cultured cells were treated with a modified Radio immunoprecipatation Assay buffer (50 mM Tris-HCl, 150 mM NaCl, 1% NP-40, 0.5% sodium deoxycholate, 0.1% SDS, glycerol, protease inhibitor cocktail (5892970001, Roche) and PhoStop (4906845001, Roche), pH 7.4) and prepared for SDS-PAGE. Gallbladder tissues were sampled according to a previously reported method.[31] Briefly, the tissue was rapidly frozen by immersion in an acetone solution containing 10% trichloroacetic acid and 10 mM Dithiothreitol, then homogenized in a water solution containing 10% trichloroacetic acid and 10 mM Dithiothreitol and centrifuged. Pellets were washed once with acetone and twice with diethyl ether. The sample powder was dissolved completely in a urea solution (8 M urea, 23 mM glycine, 234 mM sucrose, 10.4 mM dithiothreitol, 0.02 M EDTA, and 20 mM Tris-HCl pH 8.6). The concentrations of the protein samples were measured using a Bradford protein assay (500-0006, Bio-Rad). Samples were denatured and subjected to SDS-PAGE, followed by protein transfer to Polyvinylidene Fluoride membranes for immunoblotting with primary antibodies and Horseradish Peroxidase-aggregated secondary antibodies. The primary antibodies included rabbit-anti-MYPT1 (Ab7817, Proteintech, 1:2500), rabbit-anti-phospho-MYPT1 (Thr853) (4563T, CST, 1:1000), rabbit-anti-phospho-MYPT1 (Thr696) (5163T, CST, 1:1000), and mouse anti-β-actin (A1978, Sigma, 1:5000). To visualize the reactive signals, an enhanced chemiluminescence method was used with Subpico Western Solution (31059, SUDGEN) and MaxiSignal Western Solution (51508, SUDGEN).

Statistical analysis

All statistical analyses were performed using GraphPad Prism (v8). Student *t* test was performed for two-group comparisons, and one-way ANOVA followed by Bonferroni test was performed for multiple-group comparisons. Differences between groups were considered significant at a p-value < 0.05. All data are presented as the mean $\pm$ SD unless otherwise indicated.

RESULTS

MYPT1 regulates gallbladder motility and smooth muscle contractility

To determine whether MYPT1 regulates gallbladder smooth muscle contractility, we examined the gallbladder of MYPT1-KO (*Mypt1*$^{\triangle SM/\triangle SM}$) mice. First, we measured MYPT1 expression in the homozygous (*Mypt1*$^{\triangle SM/\triangle SM}$) and hetrozygous (*Mypt1*$^{+/\triangle SM}$) mutant gallbladder. Western blot analysis showed that the MYPT1 protein level in *Mypt1*$^{\triangle SM/\triangle SM}$ gallbladder was about 20% of the control gallbladder (Figure 1A), while about 65% for *Mypt1*$^{+/\triangle SM}$gallbladder. Immunofluorescence assay for *Mypt1*$^{\triangle SM/\triangle SM}$ gallbladder showed less MYPT1 expression in the smooth muscle layer, while comparable MYPT1 expression in the epithelium (Figure 1B). In the smooth muscle of *Mypt1*$^{+/\triangle SM}$ gallbladder; however, strong signals of MYPT1 expression was detected. This observation indicated a high KO efficiency of MYPT1 in *Mypt1*$^{\triangle SM/\triangle SM}$ gallbladder smooth muscle.

We then measured the contraction properties of the mutant gallbladder smooth muscle. Under resting conditions, approximately 50% of muscle strips from 28 control mice (*Mypt1*$^{+/+}$) displayed constant peristaltic contraction, whereas only 5% of muscle strips from 20 homozygous mice displayed such spontaneous contraction. The muscle strips from heterozygote mice

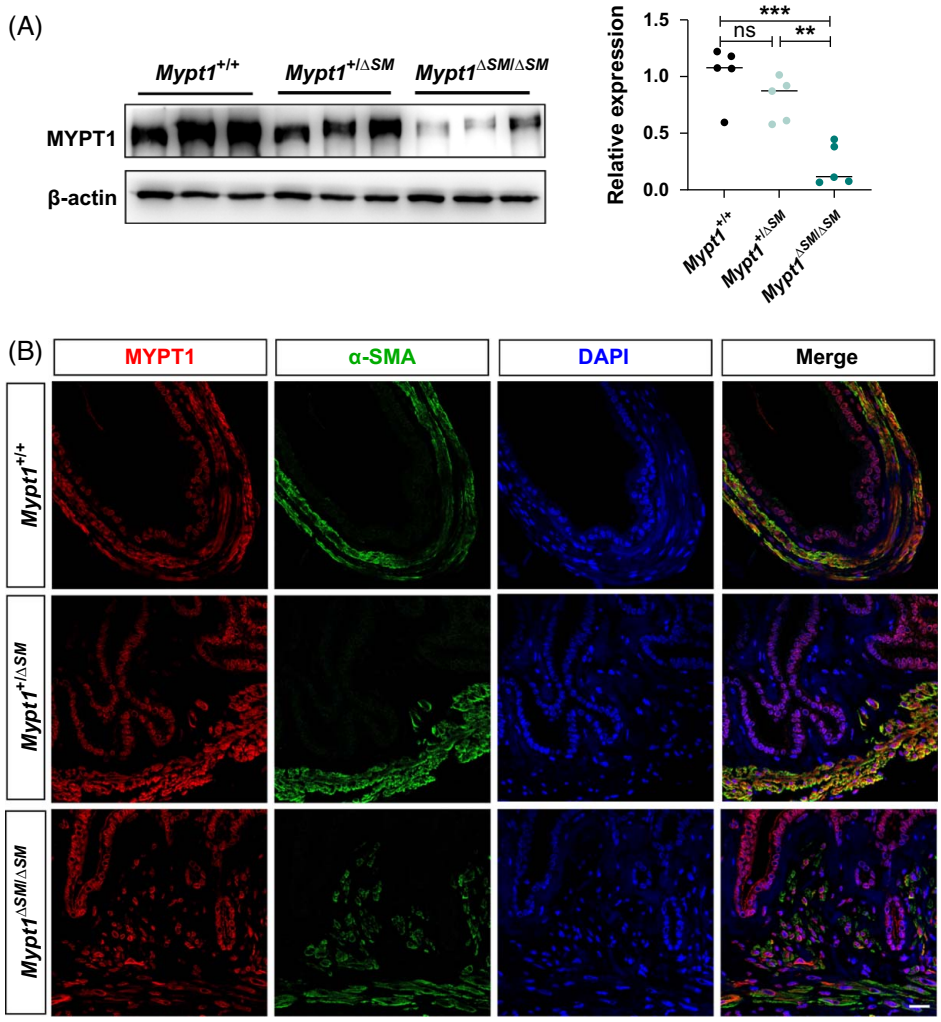

FIGURE 1 Ablation of the *Mypt1* gene results in loss of MYPT1 expression. (A) Western blot analysis of MYPT1 protein expression in gallbladders from 4-week-old *Mypt1*$^{+/+}$, *Mypt1*$^{+/\triangle SM}$, and *Mypt1*$^{\triangle SM/\triangle SM}$ mice (n = 5). The bars represent the mean values ± standard errors of the means (SEMs). *$p < 0.05$. (B) Co-immunofluorescence for MYPT1 (red) and α-SMA (green) in the gallbladder. DAPI–stained nuclei, blue. Scale bar: 20 μm. Abbreviations: MYPT1, myosin phosphatase target subunit 1; α-SMA, alpha-smooth muscle actin.

showed a reduced frequency of contractions compared with that of control mice (Figure 2A, B). Thus, ablation of MYPT1 appears to impair the spontaneous contraction of the gallbladder.

We then measured the contractile responses of the gallbladder to stimulation. For control gallbladder smooth muscle strips, stimulation with depolarization or CCK8-evoked contraction with a robust force followed by a sustained phase, which was characteristic of tonic contraction (Figure 2C, F). For the homozygote muscle strips, stimulation with Potassium Chloride evoked contraction with significantly higher maximal (0.27 ± 0.11 vs. 0.21 ± 0.08 g, $p < 0.05$) (Figure 2D) and sustained force tension than that of the control muscle strips. At the fifth minute after stimulation, the sustained tension reached 87.17% ± 6.18% of the maximal tension, which was significantly higher than that of the control (71.48% ± 12.66%, $p < 0.0001$) and heterozygote muscle (74.64% ± 8.56%, $p < 0.0001$) (Figure 2E). This result showed enhanced contraction of gallbladder smooth muscle after MYPT1 deletion, which was consistent with our previous reports showing enhanced calcium-sensitized contraction in MYPT1-deficient smooth muscles of blood vessels and intestine. To our surprise, when we stimulated the homozygote muscle strips with CCK8, the evoked maximal force was significantly lower than that of the control muscle strips ($p < 0.01$), although the relative sustained force was not altered (Figure 2G). To further confirm this phenomenon, we directly measured the gallbladder pressure *ex vivo* in response to CCK8. After we stimulated the control gallbladders by dropping CCK8 solution onto the bladder surface, the pressure increased immediately and was maintained at up to 9.3 mm Hg, while it was 7.6 mm Hg for heterozygotes and 9.58 mm Hg for homozygotes (Figure 2H). This result also supported the finding that MYPT1 deletion did not enhance the contractility of the gallbladder in response to CCK8 stimulation. CCK acts directly on CCK1 high-affinity receptors present on smooth muscle cells to stimulate contraction and likely also acts presynaptically to increase

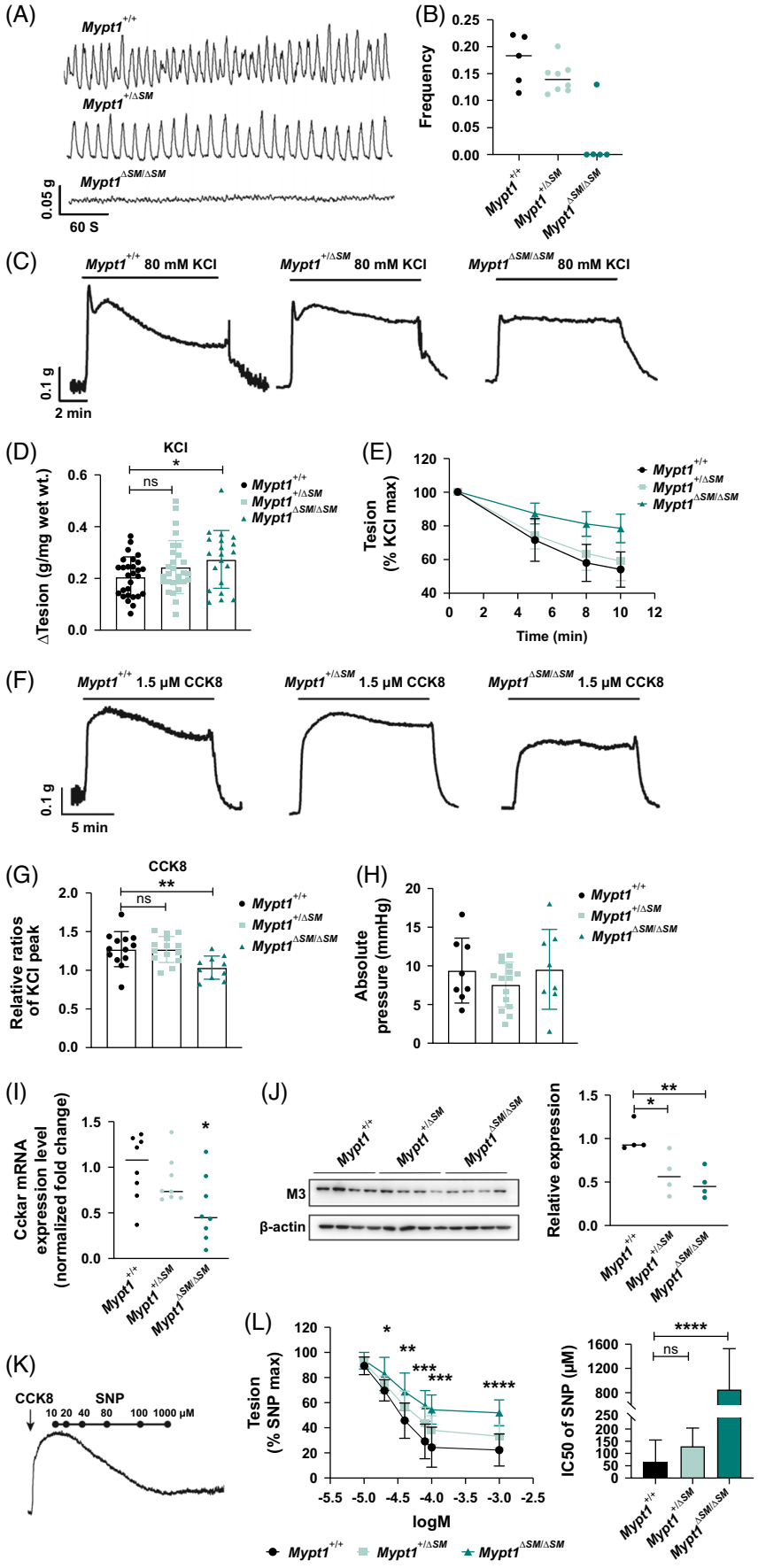
(A)
Mypt1+/+
Mypt1+/ΔSM
Mypt1ΔSM/ΔSM
0.05 g
60 S
(B)
Frequency
0.25
0.20
0.15
0.10
0.05
0.00
Mypt1+/+
Mypt1+/ΔSM
Mypt1ΔSM/ΔSM
(C)
Mypt1+/+ 80 mM KCl
Mypt1+/ΔSM 80 mM KCl
Mypt1ΔSM/ΔSM 80 mM KCl
0.1 g
2 min
(D)
KCl
ΔTesion (g/mg wet wt.)
0.6
0.4
0.2
0.0
ns
*
Mypt1+/+
Mypt1+/ΔSM
Mypt1ΔSM/ΔSM
(E)
Tesion (% KCl max)
120
100
80
60
40
0
2
4
6
8
10
12
Time (min)
Mypt1+/+
Mypt1+/ΔSM
Mypt1ΔSM/ΔSM
(F)
Mypt1+/+ 1.5 μM CCK8
Mypt1+/ΔSM 1.5 μM CCK8
Mypt1ΔSM/ΔSM 1.5 μM CCK8
0.1 g
5 min
(G)
CCK8
Relative ratios of KCl peak
2.0
1.5
1.0
0.5
0.0
ns
**
Mypt1+/+
Mypt1+/ΔSM
Mypt1ΔSM/ΔSM
(H)
Absolute pressure (mmHg)
20
15
10
5
0
Mypt1+/+
Mypt1+/ΔSM
Mypt1ΔSM/ΔSM
(I)
Cckar mRNA expression level (normalized fold change)
1.5
1.0
0.5
0.0
*
Mypt1+/+
Mypt1+/ΔSM
Mypt1ΔSM/ΔSM
(J)
Mypt1+/+
Mypt1+/ΔSM
Mypt1ΔSM/ΔSM
M3
β-actin
Relative expression
1.5
1.0
0.5
0.0
**
*
Mypt1+/+
Mypt1+/ΔSM
Mypt1ΔSM/ΔSM
(K)
CCK8
SNP
10 20 40 80 100 1000 μM
(L)
Tesion (% SNP max)
120
100
80
60
40
20
0
*
**
***
***
****
-5.5 -5.0 -4.5 -4.0 -3.5 -3.0 -2.5
logM
Mypt1+/+
Mypt1+/ΔSM
Mypt1ΔSM/ΔSM
IC50 of SNP (μM)
1600
1200
800
250
200
150
100
50
0
****
ns
Mypt1+/+
Mypt1+/ΔSM
Mypt1ΔSM/ΔSM

FIGURE 2 MYPT1-deficient gallbladder smooth muscles show altered contractile properties. (A) Representative tracings of rhythmic contractions of gallbladders from *Mypt1*$^{+/+}$, *Mypt1*$^{+/\triangle SM}$, and *Mypt1*$^{\triangle SM/\triangle SM}$ mice at the age of 4 weeks. (B) Quantification of frequency. (C and F) Representative tracings of gallbladders from 4-week-old *Mypt1*$^{+/+}$, *Mypt1*$^{+/\triangle SM}$, and *Mypt1*$^{\triangle SM/\triangle SM}$ mice elicited by 80 mM KCL or 1.5 μmol/L CCK8. (D) Maximal tension evoked by KCL treatment. (E) Quantification of dynamic alterations of sustained tension responses to treatment with 80 mM KCL. The values are represented as percentages of the peak. (G) Maximal tension responses to treatment with 1.5 μmol/L CCK8 ($n \geq 10$, $^{**}p < 0.03$). (H) Biliary pressure responses to treatment with 1.5 μmol/L CCK8 were measured at the age of 4 weeks ($n \geq 8$ for each group). (I) Quantitative RT-PCR analysis showing the mRNA levels of *Cckar*. ($n = 8$. $^{*}p < 0.05$). (J) Western blot assays and quantitative results are shown for M3 receptors in gallbladder tissues. (K) Representative trace of an isometric tension recording showing the concentration-dependent relaxation induced by SNP. (L) Log concentration-response curves for the relaxation effects of SNP expressed as a percentage of the maximal contractile response to 1.5 μmol/L CCK8. The IC50 was also calculated ($n \geq 8$, $^{****}p < 0.0001$). Abbreviations: CCK8, cholecystokinin 8; KCl, potassium chloride; MYPT1, myosin phosphatase target subunit 1; SNP, sodium nitroprusside.

acetylcholine release from vagal terminals onto gallbladder neurons, which causes smooth muscle contraction via M3 muscarinic receptors. To elucidate the possible mechanism underlying the low response to CCK8, we measured the expression of CCK8 receptor and M3 muscarinic receptors in the mutant gallbladders. The results showed that these receptors were expressed at approximately 50% lower levels than in the control gallbladders (Figure 2I, J), suggesting that the reduced response to CCK8 was due to lower receptor expression.

We then measured the relaxation property of gallbladder smooth muscle in response to nitric oxide (Figure 2K). For the control gallbladders, upon addition of different doses of a nitric oxide donor (sodium nitroprusside), the CCK8-evoked contraction was relaxed in a dose-responsive manner, and the half-maximal inhibitory concentration (IC50) value was 68.22 ± 86.96 μM (Figure 2L). For homozygote gallbladders, however, the IC50 value was significantly increased to 862.77 ± 662.44 μM ($p < 0.001$) (Figure 2L). This result clearly showed that the relaxation response of nitric oxide was heavily impaired in MYPT1-deficient gallbladders.

MYPT1-deficient gallbladders display significant hyperplasia phenotypes

The inhibited spontaneous contraction of the mutant gallbladder prompted us to examine the histology of the gallbladder. In the control gallbladders, the wall was composed of clear layers of epithelium and smooth muscle. In the heterozygous gallbladders, the bladder wall was composed of a muscle layer and an epithelial layer. In contrast to the control, both layers appeared thick and irregular possibly due to a size change of the gallbladder (Figures 1B and 3A). This alteration became more severe in the homozygous gallbladders. The boundary of the epithelium and smooth muscle layers in the 1-month-old homozygous gallbladders were distinguishable, whereas the gallbladder wall of 3-month-old homozygous mice was almost filled with hyperplastic cells. In particular, there were several cell masses of smooth muscle invading the epithelium and villi-like structures, indicating tissue remodeling or pseudo-villar projections had been formed in the wall.

We also examined the grass anatomy of the extrahepatic biliary tree of the mutant mice. The mutant bladder appeared much smaller, and the mutant bile ducts were wider and less transparent compared with the control (Figure 4A). We examined the histology of the cystic duct, common bile duct and ampulla of vater. Compared with the control, both the mutant cystic and common bile ducts showed thicker walls with hypertrophic connective tissues and comparable lumens without obstruction and intact epithelial layers visualized by CK19 staining (Figure 4B and C). The mutant ampulla of vater was composed of a smooth muscle layer that extended from intestinal smooth muscle and an intact epithelial layer, which were comparable to the control (Figure 4B and C). This result indicated that MYPT1 deletion caused wall hyperplasia of extrahepatic biliary tree, but did not affect their lumens and epithelial layers.

Above observations suggested a role of MYPT1 in tissue remodeling in addition to smooth muscle contractility. To investigate the possible mechanism underlying tissue remodeling, we first measured cytokines and hyperplasia-associated genes in mutant gallbladders. As expected, the mutant gallbladders expressed higher levels of TNF-α, TGF-β and collagens (Figure 3B–F), indicating that hyperplasia-related signaling was activated. As TGF-β signaling is believed to be the most essential signaling pathway for tissue remodeling, we thus determined the involvement of MLCP in the TGF-β response. Interestingly, upon stimulation with 10 μg/mL TGF-β for 12 hours, MYPT1-T853 and MYPT1-T696 phosphorylation levels in smooth muscle cells were elevated, although the constitutive phosphorylation of MYPT1 was also detected in resting cells (Figure 3G). Although we do not currently know the detailed regulatory scenario of MYPT1 phosphorylation in the regulation of TGF-β signaling, our results strongly suggest that the hyperplasia induced by MYPT1 ablation might be mediated through TGF-β signaling.

To further investigate the role of smooth muscle cells in regulating the remodeling processes of the gallbladder wall, we performed single-nucleus RNA sequencing analysis. Nuclei from gallbladder tissues from wild-type and KO mice, isolated as described in the methods, were subsequently sequenced by using the Illumina HiSeq X10 instrument. The transcriptional profiles of 10,239 and 15,717 cells for KO and wild-type samples, respectively,

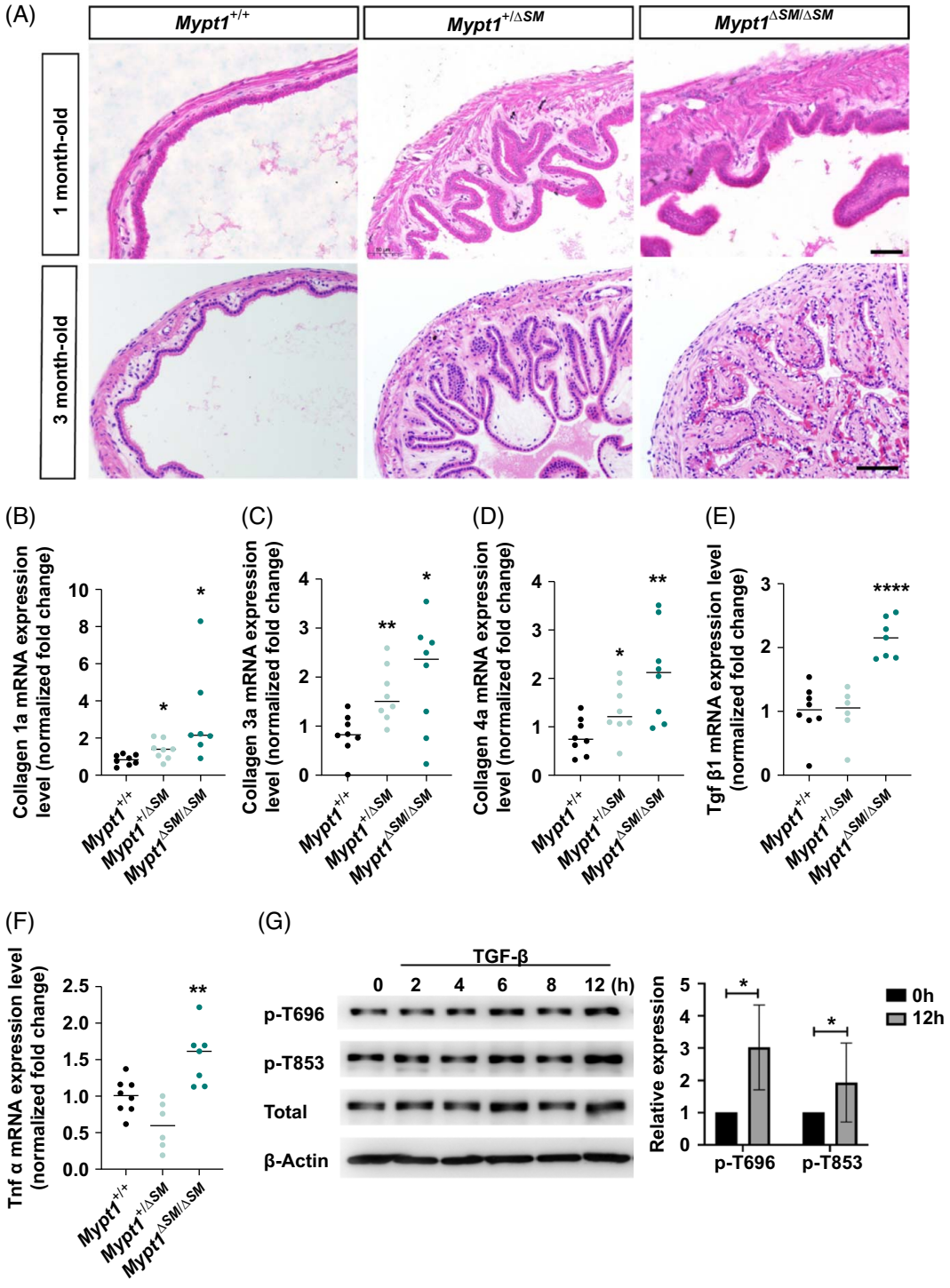

FIGURE 3 MYPT1 ablation promotes gallbladder hyperplasia. (A) The morphology of the gallbladder was tested by HE staining of longitudinal tissue sections. Scale bars: 100 μm. (B–F) Quantitative RT–PCR analysis showing the mRNA levels of *Tnfα*, *Tgfβ1*, *Col1a1*, *Col3a3*, and *Col4a1*. n > = 6. Compared with the control mice, * $p < 0.05$, * * $p < 0.01$, unpaired Student *t* test. (G) Western blot assay showing MYPT1 phosphorylation at different time points under stimulation with TGF-β. The expression levels of MYPT phosphorylation were normalized with total MYPT1. Abbreviation: MYPT1, myosin phosphatase target subunit 1.

were included in the subsequent analysis. The cell type annotations were guided by marker gene expression. Smooth muscle cell type-specific markers included well-established markers such as *Acta2*, *Mylk*, and *Myh11.* And then unsupervised clustering was performed to cluster smooth muscle cells into 6 subpopulations (Figure 5A–C). Next, we performed a Gene Ontology enrichment analysis to understand the role of each smooth muscle cell subtype. The results showed that Smooth Muscle Cell1 was mainly related to “muscle

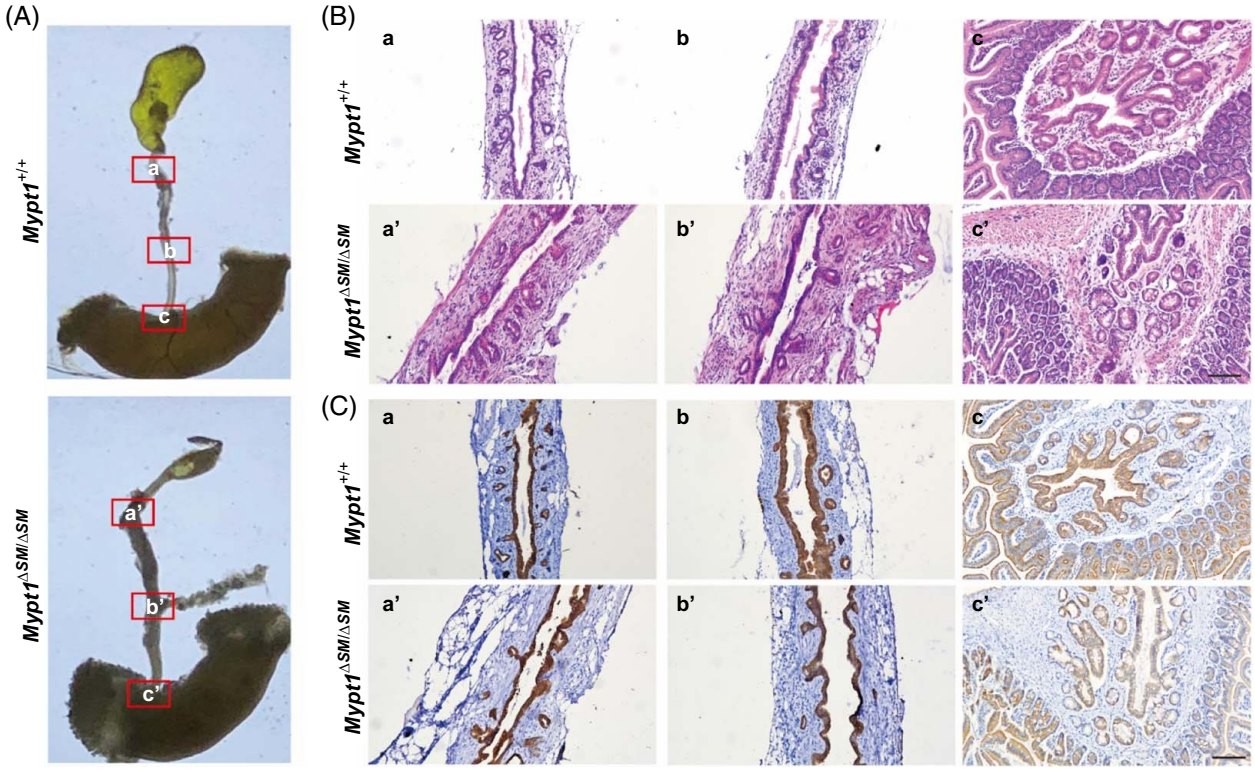

FIGURE 4 Examination of the extrahepatic bile duct system in 3-month-old mice. (A) Microscopic observation of the extrahepatic bile ducts: a, a' represent cystic duct; b, b' denote the common bile duct; c, c' illustrate the ampulla of Vater. (B) Representative images stained with hematoxylin and eosin. (C) Representative images immunolabelled with an antibody against CK19.

system process," "muscle tissue development," and "muscle contraction," suggesting that it was a contractile SMC. SMC2, SMC3, SMC4, and SMC5 all displayed downregulation of contractile relative pathways. In addition, in the KO smooth muscle, we found an extra small subset (SMC6), which was mainly associated with "regulation of neuron differentiation," "axonogenesis," "developmental cell growth," and "muscle contraction." The role of this newly identified subset in gallbladder remodeling remains to be determined. Moreover, the genes associated with cell proliferation and extracellular matrix-related signaling pathways were enriched in all subsets of mutant smooth muscle cells, which was consistent with the hyperplasia phenotype (Figure 5D, E).

Dysfunction of the MYPT1-deficient gallbladder induces CIHF in mice

To examine the complicated disorders induced by gallbladder dysfunction due to MYPT1 mutation, we examined the hepatic system in mice. In contrast to those in our previous reports,[17,32] the *Mypt1*$^{flox/flox}$ mice we used here were repeatedly crossed with Smooth Muscle Actin-Cre mice (C57BL/6 background) for approximately 10 years and thus displayed a highly homogeneous genetic background. Generally, the mutant mice (*Mypt1*$^{\triangle SM/\triangle SM}$) showed similar appearances and physiological activities except for lower body weights at 3 months after birth (Figure 6A), which may have been due to altered genetic background.

As MYPT1 can be expressed in hepatic vascular smooth muscle, MYPT1 deletion potentially affects the hepatic vascular system and hence liver function. To examine the integrity of this vascular system, we visualized the hepatic vascular system by μCT. For the mutant livers, the vascular trees were comparable to those of the controls, showing no developmental defects after MYPT1 deletion (Supplemental Figure S1, http://links.lww.com/HC9/A937). We also examined the hepatic vascular system in response to CCl4 injury. Similar to those of the controls, the mutant hepatic vessel trees also grew larger from the 12th week after injury (Supplemental Figure S1, http://links.lww.com/HC9/A937). Thus, MYPT1 deletion in smooth muscle does not seem to impair the hepatic vascular system.

HSCs play a primary role in the development of hepatic fibrosis. In a healthy liver, HSCs remain in a quiescent state. However, when fibrogenesis is triggered, quiescent HSCs undergo differentiation into activated HSCs. During this transition, they lose their intracellular lipid droplets and acquire a myofibroblastic phenotype. This is characterized by a marked increase in the expression of α-smooth muscle actin , desmin,

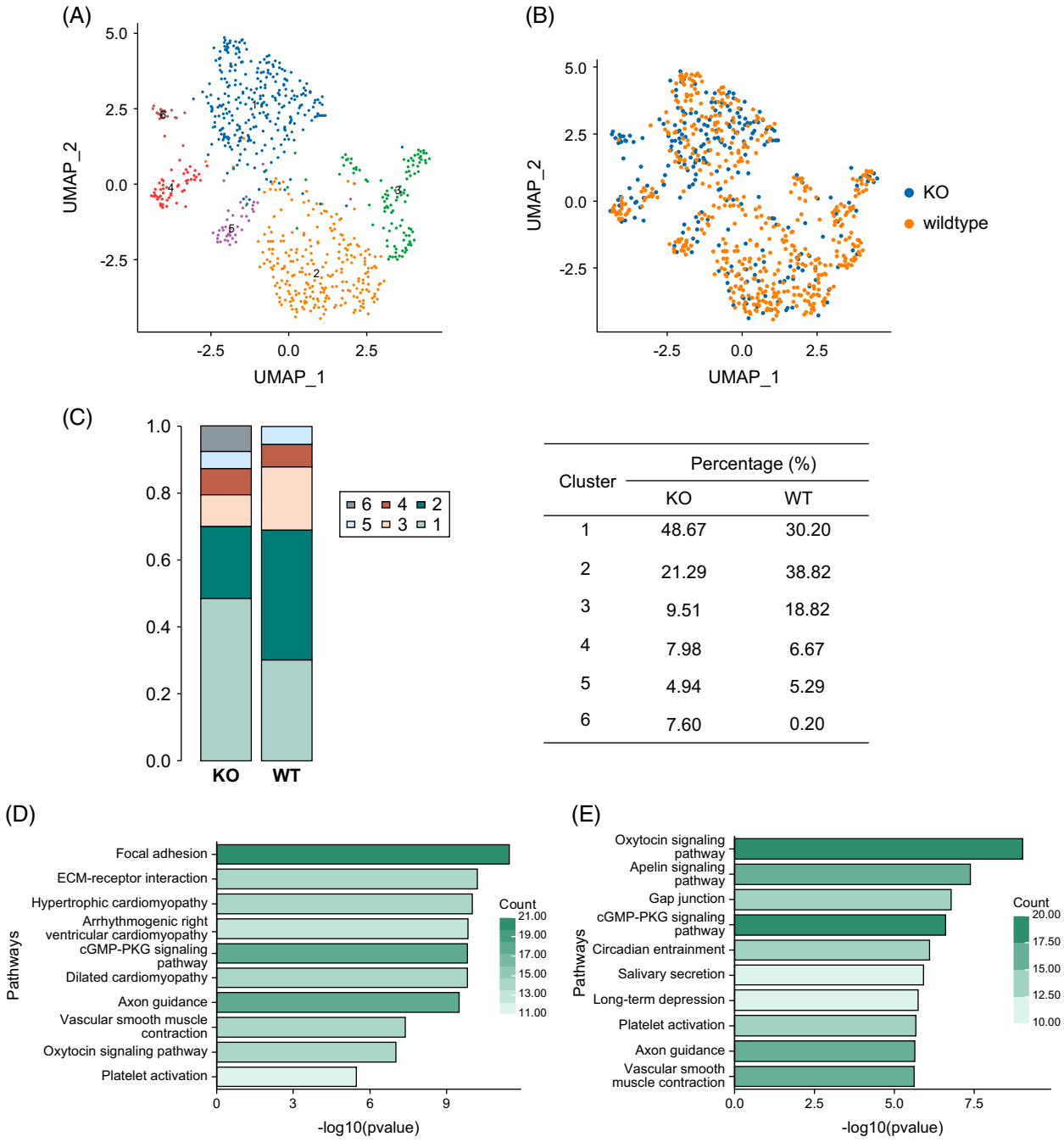

Cluster	Percentage (%)	
	KO	WT
1	48.67	30.20
2	21.29	38.82
3	9.51	18.82
4	7.98	6.67
5	4.94	5.29
6	7.60	0.20

FIGURE 5 Single-nucleus RNA sequencing analysis revealed that myosin phosphatase target subunit 1 ablation contributes to the smooth muscle cell phenotype. (A) UMAP plot of all single-nucleus RNA sequencing data showing a total of 6 distinct cell types. (B) UMAP plot of all single-nucleus RNA sequencing data based on samples. Blue represents smooth muscle cells of KO mice. Orange represents smooth muscle cells of wild-type mice. (C) Percentage of cells in each subgroup. WT: control mice; KO: homozygous mice. Top enriched pathways for gene expression changes in cluster 1 (D) and cluster 6 (E). Abbreviations: ECM, extracellular matrix; KO, knockout; PKG, protein kinase G; UMAP, uniform manifold approximation and projection; WT, wild type.

and type I collagen. Considering that our mouse model is generated by crossing *Mypt1*$^{flox/flox}$ mice crossed with transgenic mice expressing Cre driven by a smooth muscle α-actin promoter, it is important to recognize the potential role of MYPT1 in HSCs. We isolated primary HSCs from mice aged 4–6 months. Under an optical microscope, we observed that 90% of the cells contained lipid droplets. These cells were cultured in vitro for 0–6 days. At the first day (D1) of culture, the cells showed round morphology and became shuttle and star-like morphologies afterward, indicating stellate cells start to activate after the second day of culture (Supplemental Figure S2A, http://links.lww.com/HC9/A937). We also measured by western blot the MYPT1 and alpha-smooth muscle actin proteins at D0 (the day before culture), and found that D0 cells did not express

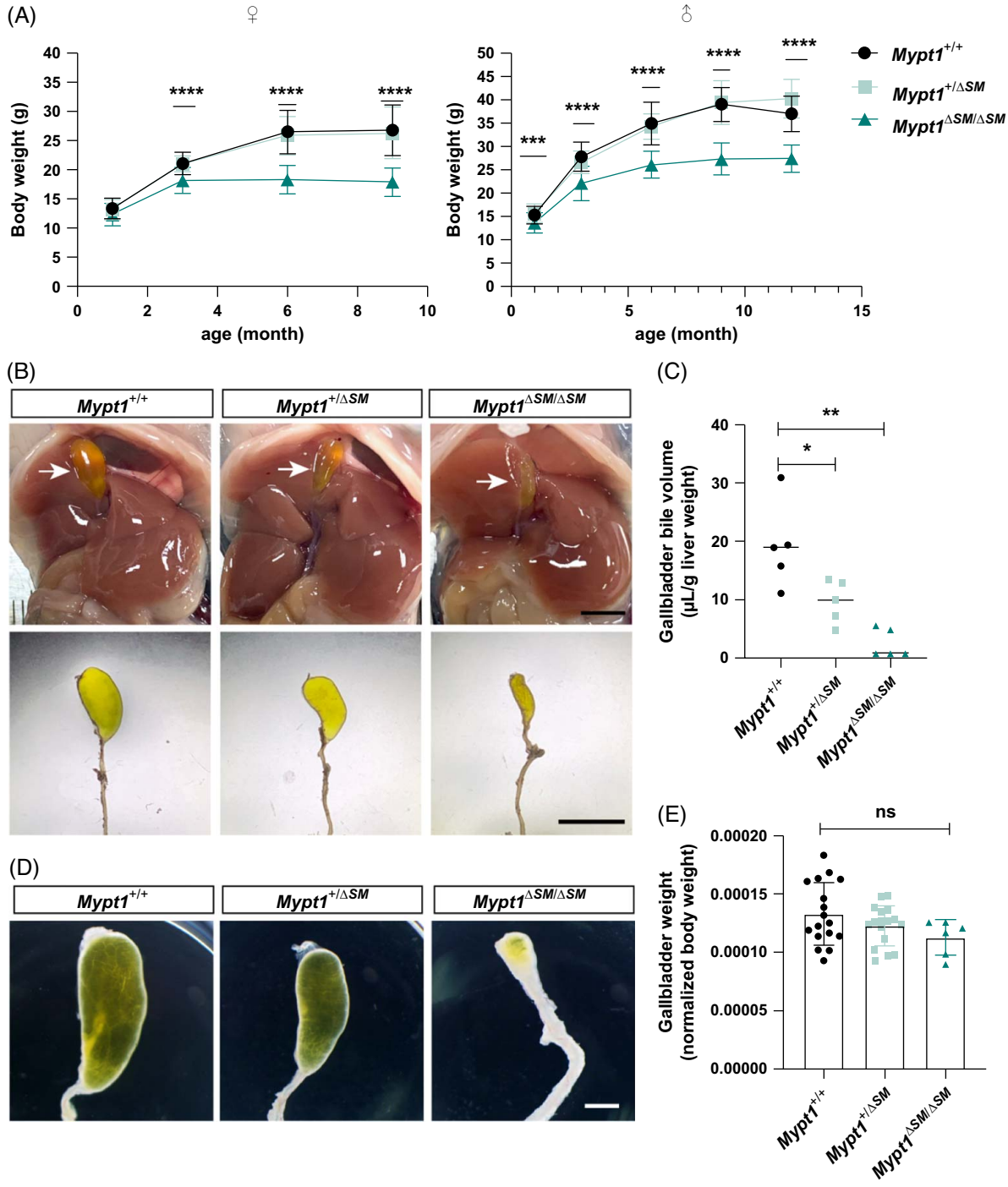

FIGURE 6 Gallbladder distension defect in *Mypt1*-KO mice. (A) Body weight at 1, 3, 6, 9, and 12 months ($n \geq 15$ for each group, each point). (B) Overnight-starved 4-week-old mice were subjected to laparotomy and macroscopic examination of the gallbladder (upper panels, arrows), and gallbladders were removed under an anatomical microscope (lower panels). Scale bars: 5 mm. (C) Quantification of bile content (*$p < 0.05$, **$p < 0.01$). (D) Microscopic observation of gallbladders from 3-month-old mice. Scale bars: 1 mm. (E) Quantification of gallbladder weight. Abbreviation: MYPT1, myosin phosphatase target subunit 1.

this protein until the fourth day after culture (Supplemental Figure S2B, http://links.lww.com/HC9/A937). This observation suggests that resting HSCs did not express MYPT1 and hence MYPT1 unlikely evolved in initiating fibrosis. However, it is important to note that we lack data to rule out its role in the later process of fibrosis.

By the age of 1 month, all groups of mice (controls, heterozygotes, and homozygotes) displayed comparable liver size and morphology. However, the gallbladders of the KO mice were apparently smaller than those of the control mice and contained much less bile solution (Figure 6B, C). At the third month after birth, the structures of the homozygous gallbladders

became tube-like, and almost no bile solution was observed (Figure 6D). This alteration was unlikely to be caused by developmental defects of the gallbladders because the gallbladder weights were not altered (Figure 6E). This observation clearly showed that the mutant gallbladders displayed impaired bile distension or bile filling.

Histologically, we examined the livers of the mutant mice at the age of 1 month. We found that 60% (6/10) of the mutant livers of homozygotes had necrotic foci in sizes of 0.31–1.36 mm^2 (0.72 ± 0.35 mm^2 on average), whereas no necrotic areas were observed in the control and heterozygote livers (Figure 7A). Interestingly, these necrotic foci disappeared 3 months after birth, indicating that this hepatic necrosis was recoverable. Measurement of hepatic fibrosis by staining with Sirius Red revealed very little fibrosis staining in the control and mutant livers before 1 month after birth. However, as the age increased to 3 months, the mutant livers showed apparent fibrosis, and the fibrosis became more extensive afterward (Figure 7B). Such fibrotic alterations were further validated by elevations in the levels of the amino acid hydroxyproline, which reflect collagen levels, in the mutant livers (Figure 7C). This result showed that MYPT1-KO mice displayed hepatic necrosis at the early stage and progressive fibrosis at the late stage. To further characterize hepatic fibrosis, we examined the biliary tracts of the mutant livers. The biliary tracts outside the liver generally appeared larger than those of the controls. The common bile ducts were generally enlarged, with their diameters increasing from 0.2 mm in the control group to 0.26 mm in the mutants ($p < 0.01$) (Figure 7D). By using an antibody against CK19, a specific marker of the biliary tract, we stained the intrahepatic biliary tracts. In the control and heterozygote livers, there were 1–3 bile ducts around the portal vein area (Figure 7E). In homozygote livers, however, the number of bile ducts increased to 28 ($p < 0.0001$) (Figure 7F). The average area of these bile ducts in the portal area-normalized portal vein area accordingly increased from 0.0284 ± 0.0230 in the control livers to 0.32 ± 0.2866 in the homozygote livers ($p < 0.0001$) (Figure 7G). This observation indicated significant hyperplasia of intrahepatic bile ducts around the central vein area in the mutant livers.

Overall, the fibrotic pathology of the mutant livers was characterized by necrosis by the age of 1 month and extensive fibrosis and hyperplastic/dilated bile ducts around the age of 6 months, which was phenotypically similar to CIHF induced by bile duct ligation in animals and to human primary CIHF. We also measured the serum parameters associated with hepatic fibrosis. The results showed that alanine aminotransferase, total bilirubin, and alkaline phosphatase levels were increased significantly in KO mice (Supplemental Figure S3, http://links.lww.com/HC9/A937).

MYPT1 protein expression can be downregulated under pathological conditions

Given that MYPT1 ablation leads to CIHF phenotypes, the factors inhibiting MYPT1 expression presumably associated with CIHF. To investigate these potential factors, we examined the effects of lipopolysaccharide (LPS) and various therapeutic drugs on MYPT1 expression because these factors have more opportunities to target gallbladder. We incubated fresh gallbladders with LPS and then measured MYPT1 protein expression by western blotting. The results showed that treatment with 100 μg/mL LPS significantly reduced MYPT1 expression (Figure 8A). We also measured the effects of 800 drugs that have been approved by the Food and Drug Administration on MYPT1 expression in A7r5 cells. We observed that approximately 60 drugs (5 μM) could downregulated the expression of MYPT1 protein by $> 50\%$ (Figure 8B). The drugs are listed in Supplemental Table S2, http://links.lww.com/HC9/A937. This effect might not have been due to the cytotoxicity of the drugs because they displayed no toxic effects on the cells at the concentration used. This observation suggests that MYPT1 expression might be downregulated by several factors, including LPS and some therapeutic drugs.

DISCUSSION

To investigate the relationship between gallbladder function and hepatic disease, we applied an animal model showing gallbladder dysfunction established by smooth muscle-specific deletion of the *Mypt1* gene. The dysfunctional gallbladders exhibited impaired motility and bile filling resulting from abolished spontaneous contraction, impaired relaxation by nitric oxide, and apparent tissue remodeling. Analysis of this animal model revealed that gallbladder dysfunction induced substantial hepatic phenotypes resembling CIHF. This finding provides a causal link between gallbladder function and liver disorders. According to our observations, we propose a mechanistic working model for gallbladder-related regulation of liver disorders under pathological conditions. Under pathological conditions such as exposure to LPS and drugs, gallbladder smooth muscle degrades the MYPT1 protein via the ubiquitin pathway.[33] As a result, the contractile properties of the gallbladder are altered, eg, spontaneous contraction is inhibited, Ca^{2+}-sensitized contraction is enhanced, and the relaxation response to nitric oxide is impaired. These alterations change the gallbladder motility necessary for bile filling and elimination, thereby leading to overfilling or leaking of the bile solution both in both biliary tracts and intrahepatic tissues. The detained bile induces necrosis of hepatic cells followed by progressive fibrosis and hyperplasia of bile ducts. As this

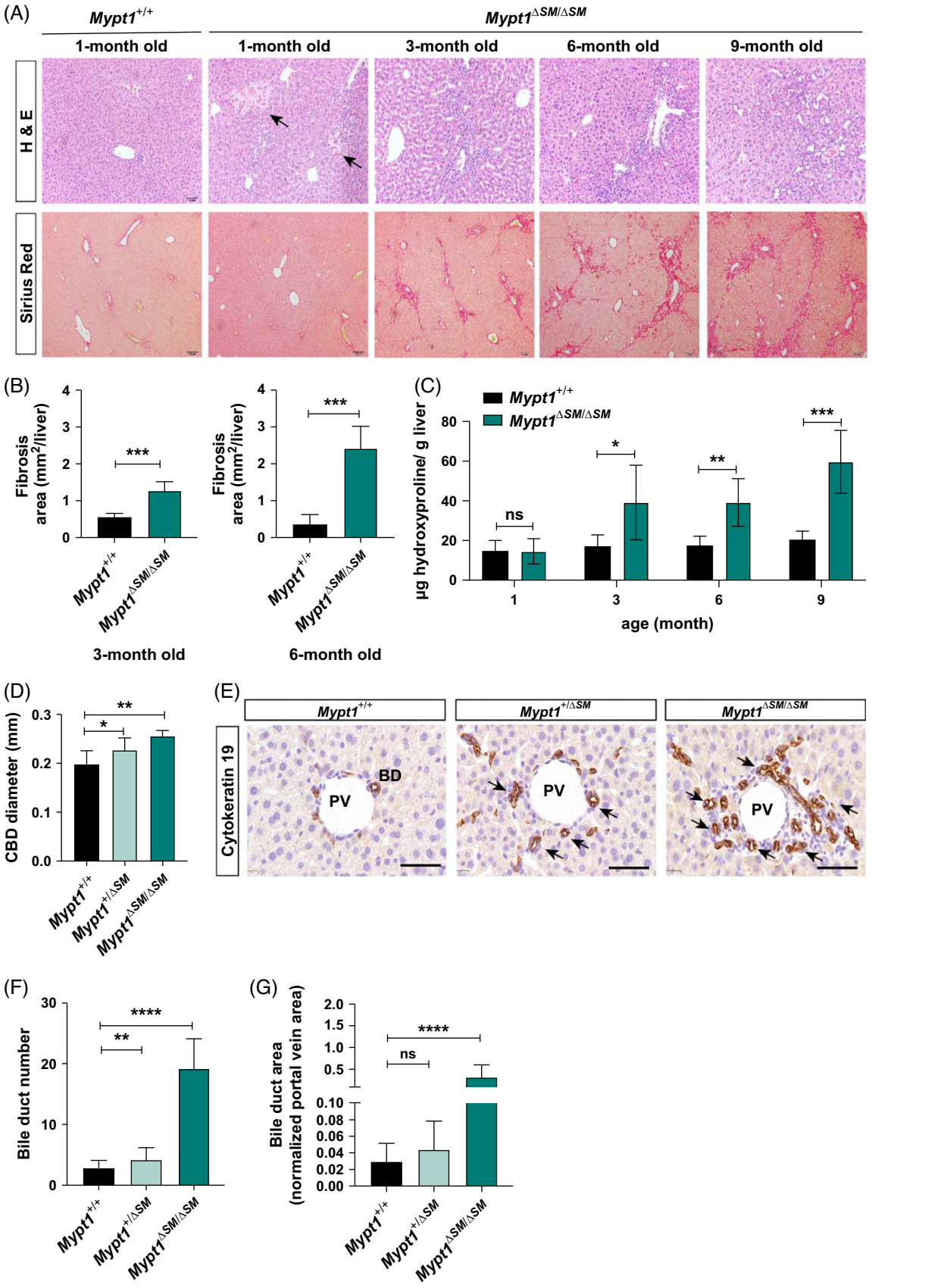

FIGURE 7 MYPT1-deficient mice display cholestasis-induced hepatic fibrosis. (A) Representative liver sections of control mice and *Mypt1*-KO mice were stained with H&E (upper) or Sirius Red (lower). Arrows indicate hepatocellular necrosis. (B) Quantification of Sirius Red staining ($n > = 3$). (C) Hepatic collagen content was measured by biochemical determination of hydroxyproline content ($n = 6$). (D) Diameter of the

extrahepatic common bile ducts from 4-week-old male mice (n = 5). (E) Representative images of liver sections from 3-month-old mice immunolabelled with an antibody against CK19. Arrows indicate bile ducts. (F) Numbers and (G) sizes of intrahepatic bile ducts surrounding portal areas (n = 5). *$p < 0.05$, **$p < 0.03$, *** $p < 0.0005$, ****$p < 0.0001$. The values are means ± SEMs. Scale bars: 50 μm. Abbreviations: BD, bile duct; H&E, hematoxylin and eosin; MYPT1, myosin phosphatase target subunit 1; LPS, lipopolysaccharide; PV, portal vein.

disorder is phenotypically similar to CIHF, we suggest that MYPT1-mediated gallbladder dysfunction may be an essential factor for CIHF.

Clinical CIHF is a syndrome caused by cholestasis, and the most representative cholestasis liver diseases include primary biliary cirrhosis and primary sclerosing cholangitis).

Despite of the pathogenesis heterogeneity proposed, both primary biliary cirrhosis and primary sclerosing cholangitis display progressive structural damages of the intrahepatic biliary tree and hence cholestasis[34] in which multiple factors including autoimmune inflammation and environmental factors may target biliary epithelial cells.[35,36] Thus, these diseases are usually considered as autoimmune disease.[37] In this report, we specifically deleted MYPT1 of smooth muscle and targeted bile flow through regulating gallbladder motility without affection of other types of cells. Resultant dysfunctional motility sufficiently alters the intrahepatic biliary tree and hence bile fibrosis. Interestingly, the main extrahepatic biliary with spare smooth muscle fibers also shows altered histology. We thus speculate that the damage from abnormal bile flow may be an initial event of cholestasis-mediated pathology, and autoimmune responses or histological alteration of bile tree might be secondary to this initial event. Although this proposal requires evidence from human observations, it provides with instructive clue to understand the ethology of cholestasis-related diseases.

MYPT1 is the main regulator of MLCP, and the binding of MYPT1 to protein phosphatase 1c increases MLCP catalytic activity by ~1000-fold.[38] In smooth muscle cells, deletion of MYPT1 leads to minimization of MLCP activity and maximization of Ca^{2+}-sensitized contraction, thereby enabling smooth muscle to produce enhanced tension force. However, we observed no enhancement of tension force produced by gallbladder smooth muscle in response to CCK8. This conflicting effect was attributable to reduced expression of the CCK8 receptor as well as tissue remodeling of the gallbladder. The tissue remodeling also suggests an alternative role of MLCP in gallbladder smooth muscle beyond Ca^{2+} sensitization. In this study, we found that stimulation with TGF-β promoted MYPT1T696/853 phosphorylation in cultured smooth muscle cells, and the expression of cytokines and remodeling-associated genes in MYPT1-deficient gallbladders was accordingly altered. This evidence clearly shows the involvement of MLCP in regulating the hyperplasia-associated gene expression network, particularly in gallbladder smooth muscle cells. The underlying regulatory mechanism remains to be determined. A possible scenario might involve the phosphorylation of G protein-coupled receptors or chromatin during the cytokine response processes.[39,40]

In summary, based on our observations, we propose a working model for the induction of hepatic fibrosis by MYPT1 downregulation. The reduction in MLCP activity

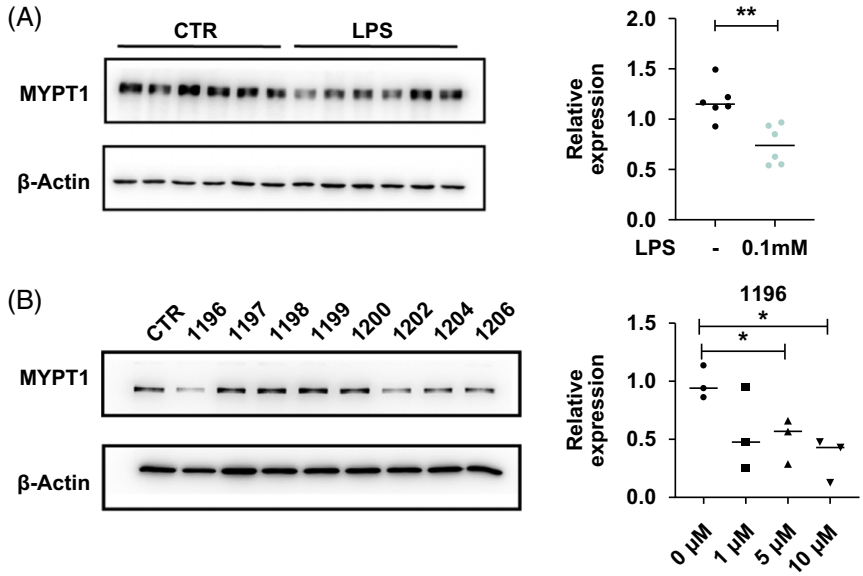

FIGURE 8 MYPT1 protein levels can be downregulated under pathological conditions. (A) LPS induced downregulation of MYPT1 expression in gallbladder tissue. n = 6, ** $p < 0.01$, unpaired Student's t test. (B) Western blotting was used to detect the effect of drugs on the expression of MYPT1 in the A7r5 cell line (representative figure). Abbreviation: MYPT1, myosin phosphatase target subunit 1.

enhances contractile responses to CCK8 and other stimuli and inhibits spontaneous contraction. The altered motility impairs bile collection and hence leads to hepatic damage and fibrosis. Simultaneously, the reduction in MYPT1 dysregulates proliferation-associated signaling cascades (eg, TGF-β), thereby promoting gallbladder proliferation and remodeling that exacerbate the process of hepatic damage.

AUTHOR CONTRIBUTIONS

Ye Wang, Min-Sheng Zhu, Xin Chen, and Xue-Na Zhang designed research studies. Ye Wang, Zhi-Hui Jiang, and Xue-Na Zhang performed experiments and acquired data. Ye Wang, Yu-Wei Zhou, Tian-Tian Qiu, and Han Wang analyzed data and results. Ye Wang, Min-Sheng Zhu, and Xue-Na Zhang wrote the manuscript. Min-Sheng Zhu, Xin Chen, and Xue-Na Zhang conducted experiments.

ACKNOWLEDGMENTS

The authors thank Dr Jun Chen and Dr Lei Xu from Nanjing Drum Tower Hospital for their assistance in liver histological analysis. The authors also thank Singleron Biotechnologies (Nanjing, China) for providing single-nucleus RNA sequencing and Jiaxin Xiong for her assistance and technical support in data analysis.

FUNDING INFORMATION

This study was supported by National Natural Science Foundation of China Grants (2022YFF0710800, 32071121 and 82192862) and the Joint Open Project of Jiangsu Key Laboratory for Pharmacology and Safety Evaluation of Chinese Materia Medica and Yangtze River Pharmaceutical Group (No. JKLPSE202004).

CONFLICTS OF INTEREST

The authors have no conflicts to report.

ORCID

Min-Sheng Zhu https://orcid.org/0000–0003–3256–6861
Xin Chen https://orcid.org/0000–0003–3304–8943
Xue-Na Zhang https://orcid.org/0000–0002–3449–3320

REFERENCES

1. Wilkins T, Agabin E, Varghese J, Talukder A. Gallbladder dysfunction: Cholecystitis, choledocholithiasis, cholangitis, and biliary dyskinesia. Prim Care. 2017;44:575–97.
2. Di Ciaula A, Wang DQ, Portincasa P. An update on the pathogenesis of cholesterol gallstone disease. Curr Opin Gastroenterol. 2018;34:71–80.
3. Kim HS, Cho SK, Kim CS, Park JS. Big data and analysis of risk factors for gallbladder disease in the young generation of Korea. PLoS One. 2019;14:e0211480.
4. Chen YK, Yeh JH, Lin CL, Peng CL, Sung FC, Hwang IM, et al. Cancer risk in patients with cholelithiasis and after cholecystectomy: a nationwide cohort study. J Gastroenterol. 2014;49:923–31.
5. Li T, Wang SK, Zhi XT, Zhou J, Dong ZR, Zhang ZL, et al. Cholecystectomy is associated with higher risk of early recurrence and poorer survival after curative resection for early stage hepatocellular carcinoma. Sci Rep. 2016;6:28229.
6. Martin DJ, Weideman R, Crook T, Brown G. Relationship of hepatic fibrosis, cirrhosis, and mortality with cholecystectomy in patients with hepatitis C virus infection. Eur J Gastroenterol Hepatol. 2016;28:181–6.
7. Xie ZQ, Li HX, Tan WL, Yang L, Ma XW, Li WX, et al. Association of cholecystectomy with liver fibrosis and cirrhosis among adults in the USA: A population-based propensity score-matched study. Front Med (Lausanne). 2021;8:787777.
8. Housset C, Chrétien Y, Debray D, Chignard N. Functions of the gallbladder. Compr Physiol. 2016;6:1549–77.
9. Shaffer EA. Review article: Control of gall-bladder motor function. Aliment Pharmacol Ther. 2000;14(suppl 2):2–8.
10. Niebergall-Roth E, Teyssen S, Singer MV. Neurohormonal control of gallbladder motility. Scand J Gastroenterol. 1997;32:737–50.
11. Behar J, Mawe GM, Carey MC. Roles of cholesterol and bile salts in the pathogenesis of gallbladder hypomotility and inflammation: cholecystitis is not caused by cystic duct obstruction. Neurogastroenterol Motil. 2013;25:283–90.
12. Hernández-Moreno D, Morales S, Camello-Almaraz C, Pozo MJ, Camello PJ. Monochloramine effects on gallbladder contractility. Clin Exp Pharmacol Physiol. 2021;48:597–604.
13. Somlyo AP, Somlyo AV. Signal transduction and regulation in smooth muscle. Nature. 1994;372:231–6.
14. He WQ, Peng YJ, Zhang WC, Lv N, Tang J, Chen C, et al. Myosin light chain kinase is central to smooth muscle contraction and required for gastrointestinal motility in mice. Gastroenterology. 2008;135:610–20.e2.
15. Kuo IY, Ehrlich BE. Signaling in muscle contraction. Cold Spring Harb Perspect Biol. 2015;7:a006023.
16. Ito M, Nakano T, Erdödi F, Hartshorne DJ. Myosin phosphatase: Structure, regulation and function. Mol Cell Biochem. 2004;259:197–209.
17. He WQ, Qiao YN, Peng YJ, Zha JM, Zhang CH, Chen C, et al. Altered contractile phenotypes of intestinal smooth muscle in mice deficient in myosin phosphatase target subunit 1. Gastroenterology. 2013;144:1456–65.e5; 1465 e1-5.
18. Zhang CH, Wang P, Liu DH, Chen CP, Zhao W, Chen X, et al. The molecular basis of the genesis of basal tone in internal anal sphincter. at Commun. 2016;7:11358; 1358.
19. Schjoldager BT. Role of CCK in gallbladder function. Ann N Y Acad Sci. 1994;713:207–18.
20. Luman W, Ardill JE, Armstrong E, Smith GD, Brett L, Lessells AM, et al. Nitric oxide and gall-bladder motor function. Aliment Pharmacol Ther. 1998;12:425–32.
21. Gultekin H, Erdem SR, Emre-Aydingoz S, Tuncer M. The role of nitric oxide in the electrical field stimulation-induced contractions of sphincter of oddi and gallbladder strips in Guinea pigs. J Pharmacol Sci. 2006;101:240–4.
22. Lu LG CC, Cheng J. Consensus on the diagnosis and treatment of cholestatic liver diseases(2015). Chin J Hepatol. 2015;23:924–33.
23. Pollock G, Minuk GY. Diagnostic considerations for cholestatic liver disease. J Gastroenterol Hepatol. 2017;32:1303–9.
24. Mariotti V, Cadamuro M, Spirli C, Fiorotto R, Strazzabosco M, Fabris L. Animal models of cholestasis: An update on inflammatory cholangiopathies. Biochim Biophys Acta Mol Basis Dis. 2019;1865:954–64.
25. Parkman HP, Bogar LJ, Bartula LL, Pagano AP, Thomas RM, Myers SI. Effect of experimental acalculous cholecystitis on gallbladder smooth muscle contractility. Dig Dis Sci. 1999;44:2235–43.
26. Alcón S, Morales S, Camello PJ, Hemming JM, Jennings L, Mawe GM, et al. A redox-based mechanism for the contractile

and relaxing effects of NO in the guinea-pig gall bladder. J Physiol. 2001;532:793–810.
27. Song K, Zhong XG, Xia XM, Huang JH, Fan YF, Yuan RX, et al. Orai1 forms a signal complex with SK3 channel in gallbladder smooth muscle. Biochem Biophys Res Commun. 2015;466:456–62.
28. Heinrich S, Georgiev P, Weber A, Vergopoulos A, Graf R, Clavien PA. Partial bile duct ligation in mice: A novel model of acute cholestasis. Surgery. 2011;149:445–51.
29. Liao Y, Smyth GK, Shi W. featureCounts: An efficient general purpose program for assigning sequence reads to genomic features. Bioinformatics. 2014;30:923–30.
30. Yu G, Wang LG, Han Y, He QY. clusterProfiler: An R package for comparing biological themes among gene clusters. OMICS. 2012;16:284–7.
31. Sun J, Tao T, Zhao W, Wei L, She F, Wang P, et al. CPI-17-mediated contraction of vascular smooth muscle is essential for the development of hypertension in obese mice. J Genet Genomics. 2019;46:109–8.
32. Qiao YN, He WQ, Chen CP, Zhang CH, Zhao W, Wang P, et al. Myosin phosphatase target subunit 1 (MYPT1) regulates the contraction and relaxation of vascular smooth muscle and maintains blood pressure. J Biol Chem. 2014;289:22512–3.
33. Zhao W, Wang P, He W, Tao T, Li H, Li Y, et al. MYPT1 down-regulation by lipopolysaccharide-SIAH1/2 E3 ligase-ubiquitin-proteasomal degradation contributes to colonic obstruction of hirschsprung disease. Cell Mol Gastroenterol Hepatol. 2020;9:345–7 e6.
34. Pinzani M, Luong TV. Pathogenesis of biliary fibrosis. Biochim Biophys Acta Mol Basis Dis. 2018;1864(4 Pt B):1279–83.
35. Gulamhusein AF, Hirschfield GM. Primary biliary cholangitis: pathogenesis and therapeutic opportunities. Nat Rev Gastroenterol Hepatol. 2020;17:93–110.
36. Sarcognato S, Sacchi D, Grillo F, Cazzagon N, Fabris L, Cadamuro M, et al. Autoimmune biliary diseases: Primary biliary cholangitis and primary sclerosing cholangitis. Pathologica. 2021;113:170–84.
37. Younossi ZM, Bernstein D, Shiffman ML, Kwo P, Kim WR, Kowdley KV, et al. Diagnosis and management of primary biliary cholangitis. Am J Gastroenterol. 2019;114:48–63.
38. Chen CP, Chen X, Qiao YN, Wang P, He WQ, Zhang CH, et al. In vivo roles for myosin phosphatase targeting subunit-1 phosphorylation sites T694 and T852 in bladder smooth muscle contraction. J Physiol. 2015;593:681–700.
39. Shuhaibar LC, Kaci N, Egbert JR, Horville T, Loisay L, Vigone G, et al. Phosphatase inhibition by LB-100 enhances BMN-111 stimulation of bone growth. JCI Insight. 2021;6:e141426.
40. Takahashi H, Yang G, Yoneshiro T, Abe Y, Ito R, Yang C, et al. MYPT1-PP1beta phosphatase negatively regulates both chromatin landscape and co-activator recruitment for beige adipogenesis. Nat Commun. 2022;13:5715.

How to cite this article: Wang Y, Jiang Z-H, Zhou Y-W, Qiu T-T, Wang H, Zhu M-S, et al. Gallbladder dysfunction caused by MYPT1 ablation triggers cholestasis-induced hepatic fibrosis in mice. Hepatol Commun. 2024;8:e0473. https://doi.org/10.1097/HC9.0000000000000473